Hydrophobic Hydration: A Free Energy Perturbation Study

B. G. Rao and U. C. Singh*

Contribution from the Department of Molecular Biology, Scripps Clinic and Research Foundation, La Jolla, California 92037. *Received August 26, 1988*

Abstract: Differences in free energy of hydration between molecules within a class of chemical compounds, such as normal alkanes, tetraalkylmethanes, alkyl- and tetraalkylammonium ions, amines and aromatic compounds, have been calculated by a coordinate coupled free energy perturbation method. The calculated free energy differences agree reasonably well with the experimental values. The patterns of variation of free energy change with coupling parameter λ are found to differ for different classes of compounds. These results are interpreted in terms of the differing hydration processes of these molecules. Hydrophobic hydration of hydrocarbons and ammonium ions bearing large hydrocarbon groups seems to result from tightly bound water structure around the solute. In contrast, the water structure around amines and aromatic compounds bearing polar functional groups is dictated by the directional hydrogen bonding of the polar group with water. The direction of the free energy change seems to be dictated by solute–solvent interaction energy, which has major contribution to free energy change for alkyl-substituted ammonium ions.

Hydrophobic hydration has an important effect on macromolecular conformations, biological and artificial membrane organization, micelle formation, and such technological processes as solubilization, extraction, and phase-transfer catalysis.[1-3] The most striking manifestation of hydrophobic hydration is large, negative, and solute-size dependent entropies of solution.[4] Also associated with this process is a decrease in volume that leads to a compact solvent structure. Since Eley's first proposal of a cavity model[5] and Frank and Evans' classic structural hypothesis[4] of hydrophobic solvation, an increasingly large number of studies[6] has been made to elucidate the origin of this phenomena. According to Frank and Evans' hypothesis, the interaction of apolar solutes with water enhances hydrogen bonding between the surrounding water molecules and induces formation of a kind of "cooperative" ice-like, but labile, water structure, which causes the decrease in entropy and molar volume. This view has been supported by a large number of structural, kinetic and spectroscopic investigations.[7] However, several molecular details and mechanistic aspects of hydrophobic hydration remain to be elucidated.

Computer simulations have been widely employed[8-15] to study the hydration phenomenon. These initial studies showed that water surrounding an apolar solute molecule forms strongly hydrogen-bonded framework resembling that of a crystalline clathrate hydrate. Such a structure is suggested to be stable from the calculated interaction energies. However, free energy is a better measure of the thermodynamic stability of a system than interaction energy. Recent computer simulation studies, therefore, attempted to calculate differences in free energies of hydration for closely related systems.[16-20] Subsequent to these developments, Singh et al.[21,22] showed that differences in Gibbs free energy of hydration of two quite dissimilar systems can be computed very accurately by molecular dynamics simulation using "free energy perturbation approach". In several other recent studies[23-25] free energy of hydration for simple solutes were calculated with Monte Carlo simulations. These free energy simulation methods have also been employed[26-31] to study such diverse problems as enzyme catalysis, enzyme inhibition, nucleic acid tautomerism, molecular association, and drug design. Therefore, this method seems to be suitable to study a complex phenomenon such as hydrophobic hydration.

We report here a detailed study of hydration of solute molecules bearing both polar and apolar moieties, e.g., normal alkanes, tetraalkylmethane molecules, amines, ammonium ions, and aromatic compounds. Further, we show that these simulation studies can be very useful in understanding many factors contributing to hydration process. Since only differences in free energy between two related systems can be calculated by the free energy perturbation approach, we simulated transformations of a higher homologue to a lower homologue within a class of compounds. Among hydrocarbons we chose to transform $C_2H_6 \rightarrow CH_4$, $C_3H_8 \rightarrow C_2H_6$, and $C_4H_{10} \rightarrow C_3H_8$. The transformations of amines

(1) Dogonadze, R. R.; Kornyshev, A. A.; Ulstrup, J. *The Chemical Physics of Solvation*; Dogonadze, R. R., Kalman, E., Kornyshev, A. A., Ulstrup, J., Eds.; Elsevier: Amsterdam, 1985; Part A, Theory of Solvation, Chapter 1, p 3.
(2) Tanford, C. *The Hydrophobic Effect: Formation of Micelles and Biological Membranes*; John Wiley & Sons: New York, 1980.
(3) Ben-Naim, A. *Water and Aqueous Solutions—Introduction to Molecular Theory*; Plenum: New York, 1974.
(4) Frank, H. S.; Evans, M. W. *J. Chem. Phys.* **1945**, *13*, 507.
(5) Eley, D. D. *Trans. Faraday Soc.* **1939**, *35*, 1421.
(6) Franks, F. *Faraday Symp. Chem. Soc.* **1982**, *17*, 7.
(7) Huot, J. Y.; Jolicoeur, C. *The Chemical Physics of Solvation*; Dogonadze, R. R., Kalman, E., Kornyshev, A. A., Ulstrup, J., Eds.; Elsevier: Amsterdam, 1985; Part A, Theory of Solvation, Chapter 11, p 417 and the references cited therein.
(8) Nemethy, G.; Scheraga, H. A. *J. Chem. Phys.* **1962**, *36*, 3382, 3401.
(9) Owicki, J. C.; Scheraga, H. A. *J. Am. Chem. Soc.* **1977**, *99*, 7413.
(10) Geiger, A.; Rahaman, A.; Stillinger, F. M. *J. Chem. Phys.* **1979**, *70*, 263.
(11) Pangali, C.; Rao, M.; Berne, B. J. *J. Chem. Phys.* **1979**, *71*, 2975.
(12) Swaminathan, S.; Harrison, S. W.; Beveridge, D. L. *J. Am. Chem. Soc.* **1978**, *100*, 4392.
(13) Swaminathan, S.; Beveridge, D. L. *J. Am. Chem. Soc.* **1979**, *101*, 5832.
(14) Okazaki, S.; Nakanishi, K.; Touhara, H.; Adachi, Y. *J. Chem. Phys.* **1979**, *71*, 2421.
(15) Ravishanker, G.; Mehrotra, P. K.; Mezei, M.; Beveridge, D. L. *J. Am. Chem. Soc.* **1984**, *106*, 4102.
(16) Postma, J. P. M.; Berendsen, H. J.; Haak, J. R. *Faraday Symp.* **1981**, *17*, 55.
(17) Jorgensen, W. L.; Ravimohan, C. *J. Chem. Phys.* **1985**, *83*, 3050.
(18) Lybrand, T. P.; McCammon, J. A.; Wipff, G. *Proc. Natl. Acad. Sci. U.S.A.* **1986**, *83*, 833.
(19) Wong, C. F.; McCammon, J. A. *J. Am. Chem. Soc.* **1986**, *108*, 3830.
(20) Straatsma, T. P.; Berendsen, H. J. C.; Postma, J. P. M. *J. Chem. Phys.* **1986**, *85*, 6720.
(21) Singh, U. C.; Brown, F. K.; Bash, P. A.; Kollman, P. A. *J. Am. Chem. Soc.* **1987**, *109*, 1607.
(22) Bash, P. A.; Singh, U. C.; Langridge, R.; Kollman, P. A. *Science* **1987**, *236*, 564.
(23) Jorgensen, W. L.; Buckner, J. K.; Huston, S. E.; Rossky, P. J. *J. Am. Chem. Soc.* **1987**, *109*, 1891.
(24) Jorgensen, W. L.; Briggs, J. M.; Gao, J. *J. Am. Chem. Soc.* **1987**, *109*, 6857.
(25) Migliore, M.; Corongiu, G.; Clementi, E.; Lie, G. C. *J. Chem. Phys.* **1988**, *88*, 7766.
(26) Bash, P. A.; Singh, U. C.; Brown, F. K.; Langridge, R.; Kollman, P. A. *Science* **1987**, *235*, 574.
(27) Rao, S.; Singh, U. C.; Bash, P. A.; Kollman, P. A. *Nature* **1987**, *328*, 551.
(28) Singh, U. C. *Proc. Natl. Acad. Sci. U.S.A.* **1988**, *85*, 4280.
(29) Singh, U. C.; Benkovic, S. J. *Proc. Natl. Acad. Sci. U.S.A.* **1988**, *85*, 9519.
(30) Cieplak, P.; Kollman, P. A. *J. Am. Chem. Soc.* **1988**, *110*, 3734.
(31) Reynolds, C. A.; King, P. M.; Richards, W. G. *Nature* **1988**, *334*, 80.

0002-7863/89/1511-3125$01.50/0

include $Me_3N \rightarrow Me_2NH$, $Me_2NH \rightarrow MeNH_2$, and $MeNH_2 \rightarrow NH_3$, the solvation patterns of which change irregularly in the series.[32] However, the free energy changes expected from these transformations and those of alkanes are very small (around 1.0 kcal/mol or less), although a methyl group is mutated into a hydrogen atom in each case. Reasonably larger free energy changes are expected in the transformations of corresponding ammonium ions: $Me_3NH^+ \rightarrow Me_2NH_2^+$, $Me_2NH_2^+ \rightarrow MeNH_3^+$, and $MeNH_3^+ \rightarrow NH_4^+$. Both polar and nonpolar interactions seem to contribute to solvation of these ions. Moreover, the solvation of symmetrical tetraalkylammonium ions, which have been used as model compounds for experimental studies[33] of hydrophobic hydration, is strongly influenced by the interactions of alkyl groups with water. We report here the transformations of $Bu_4N^+ \rightarrow Pr_4N^+$, $Pr_4N^+ \rightarrow Et_4N^+ \rightarrow Me_4N^+$, and $Me_4N^+ \rightarrow NH_4^+$. For comparison, the transformations are reported for corresponding neutral hydrocarbons, namely, $Bu_4C \rightarrow Pr_4C$, $Pr_4C \rightarrow Et_4C$, $Et_4C \rightarrow Me_4C$, and $Me_4C \rightarrow CH_4$, which have purely hydrophobic contributions from the hydrocarbon groups. Finally, the transformations of some aromatic compounds studied are aniline → benzene, phenol → benzene, and toluene → benzene.

Free Energy Perturbation Method

The free energy perturbation method is based on the statistical perturbation theory developed by Zwanzig.[34] Singh et al. incorporated it into the framework of molecular dynamics as discussed in detail elsewhere.[21] The essential featues of the method are briefly described here.

The total Hamiltonian employed in this method is separated into two parts

$$H = H_0 + H_1 \tag{1}$$

where H_0 is the Hamiltonian of an unperturbed system and H_1 is the perturbation. The Gibbs free energy contribution due to the perturbation is given by

$$G_1 = -\frac{1}{\beta} \ln \langle \exp(-\beta H_1) \rangle_0 \tag{2}$$

where $\beta = 1/RT$. The average of $\exp(-\beta H_1)$ is computed over the unperturbed ensemble of the system. To obtain ΔG between two states, it is necessary to define perturbed group Hamiltonian for states A and B as

$$H_\lambda = \lambda H_A + (1 - \lambda) H_B \qquad 0 \le \lambda \le 1 \tag{3}$$

where H_A is the Hamiltonian for A, and H_B is that for B. When $\lambda = 1$, $H_\lambda = H_A$, and when $\lambda = 0$, $H_\lambda = H_B$. At intermediate values of λ, the state is a hypothetical mixture of A and B. This type of coupling ensures a smooth conversion of state A into B. Even if the two states are significantly different in chemical structure, the conversion can be made smooth by choosing smaller increments of λ and by allowing the system to equilibrate sufficiently longer after each perturbation. If the range of λ is divided into N windows, $\{\lambda_i, i = 1,N\}$, the solute state is perturbed to λ_{i+1} and λ_{i-1} states at each window λ_i, and the free energy difference between the states A and B is computed by summation over all the windows as

$$\Delta G = \sum_{i=1}^{N} G_1(\lambda_i) \tag{4}$$

In an alternative approach, called time-dependent perturbation or slow growth, the coupling parameter λ is defined as a function of time, which varies continuously, either in a linear or nonlinear fashion, as the system evolves with time. If $d\lambda$ is the increment at each time step and $d\lambda \ll 1$, then

$$G_1(\lambda) = H_1(\lambda) \tag{5}$$

The free energy difference is then simply reduced to

$$\Delta G = \sum_{\lambda} H_1(\lambda) \tag{6}$$

According to eq 6, the free energy difference between the solute states A and B is simply the sum of the perturbation energy at each λ over the entire range of λ.

Free Energy Decoupling. Some sampling difficulties arise during the transformation of a polar solute to a nonpolar solute in water when a large change in molecular volume occurs. The simultaneous mutation of the partial charges and the nonbonded parameters R and ϵ during the transformation results in solute–solvent configurations wherein some solvent molecules are too close to the solute leading to very large solute–solvent interaction energies. Even though the free energy difference should be path independent, this behavior introduces some sort of *phase transition* resulting in the introduction of path dependency into the calculation. To eliminate this artifact, the free energy is decomposed into two components called electrostatic and van der Waals components. If the total energy is written as

$$E_{tot} = E_{badh} + E_{ele} + E_{vdw} \tag{7}$$

where E_{badh} is the energy due to bond, angle, and dihedral and E_{ele} and E_{vdw} are the electrostatic and van der Waals interaction energies, respectively, then the conversion of state A to state B can be achieved through an intermediate state A′.

$$A \rightarrow A' \rightarrow B \tag{8}$$

$$\Delta G_{AB} = \Delta G_{AA'} + \Delta G_{A'B} \tag{9}$$

In state A′ the solute has the same intramolecular and van der Waals parameters as in state A. However, state A′ assumes the charge distribution of B. Thus, $\Delta G_{AA'}$ corresponds to the electrostatic contribution to the free energy difference. The conversion of A to A′ can be achieved smoothly since the van der Waals parameters are the same in both A and A′. $\Delta G_{A'B}$ is the van der Waals contribution to the free energy which includes the contribution from bond, angle, and dihedral terms in addition to the contribution from nonbonded interaction term.

Coordinate Coupling. During the mutation of a molecule, it is necessary to reset its coordinates at every intermediate state, since the coordinates of the final state differ from those of the initial state. For instance, the conversion of one hydrocarbon into another hydrocarbon, by mutation of a methyl group into a hydrogen, involves a change of a C–C bond (1.52 A) to a C–H bond (1.09 A). Therefore, for an accurate description of a molecule's geometry at an intermediate state λ between states A and B, the coordinates of the system have been coupled as

$$X_\lambda = \lambda X_A + (1 - \lambda) X_B \tag{10}$$

where X_λ, X_A, and X_B are the coordinates of the system at states λ, A, and B, respectively. Coordinate coupling has been implemented as follows. A coordinate of a system that is changing linearly along an axis is extrapolated along the defined axis for the $\lambda_{i\pm1}$ windows. If several such axes are involved, as in the case of shrinking a ring system from one size to another, an iterative method is used to satisfy all the constraints. When a rotation is involved along an axis, the coordinates of the atoms involved in the rotation are obtained by the desired rotation along the axis. The extrapolated coordinates for the $\lambda_{i\pm1}$ windows are used in calculating the interaction energies.

Computational Details

The calculations were performed with the AMBER (Version 3.1) program[35] on the CRAY X-MP/14se computer system at Scripps Clinic and Research Foundation. The molecules were built using the PREP and LINK modules of the AMBER from the known geometric information. The system was solvated with the EDIT module of the program by placing the solute molecule at the center of a rectangular box containing three cubes of 216 TIP3P water molecules[36] and discarding any water molecule farther than a distance of 12.0 Å from any atom of the solute along the

(32) Trotman-Dickinson, A. F. *J. Chem. Soc.* **1949**, 1293.
(33) Frank, H. S.; Wen, W. Y. *Discuss. Faraday Soc.* **1957**, *24*, 133.
(34) Zwanzig, R. W. *J. Chem. Phys.* **1954**, *22*, 1420.

(35) AMBER (Version 3.1) is a fully vectorized version of AMBER (Version 3.0) by Singh et al. (Singh, U. C.; Weiner, P. K.; Caldwell, J. W.; Kollman, P. A. University of California: San Francisco, 1986). AMBER (Version 3.1) also includes coordinate coupling and intra/inter decomposition.
(36) Jorgensen, W. L.; Chandrasekhar, J.; Madura, J. D. *J. Chem. Phys.* **1983**, *79*, 926.

Table I. Size of the MD Box and the Number of Solvating Water Molecules

simulation	solute	ref	x (Å)	y (Å)	z (Å)	no. of H_2O
1	C_2H_6	CH_4	26.53	25.84	26.08	523
2	C_3H_8	C_2H_6	28.24	26.85	26.08	569
3	C_4H_{10}	C_3H_8	29.07	27.31	27.10	605
4	Me_4C	CH_4	28.52	28.52	27.28	624
5	Et_4C	Me_4C	33.01	33.01	29.28	930
6	Pr_4C	Et_4C	37.53	37.53	31.35	1301
7	Bu_4C	Pr_4C	40.03	40.03	31.35	1459
8	$MeNH_2$	NH_3	26.77	26.08	25.80	518
9	Me_2NH	$MeNH_2$	27.91	26.87	25.83	552
10	Me_3N	Me_2NH	27.98	27.99	25.75	567
11	$MeNH_3^+$	NH_4^+	26.49	26.08	26.29	528
12	$Me_2NH_2^+$	$MeNH_3^+$	28.51	26.38	26.08	558
13	Me_3NH^+	$Me_2NH_2^+$	28.51	28.13	26.90	614
14	Me_4N^+	NH_4^+	26.51	26.51	25.28	496
15	Et_4N^+	Me_4N^+	31.01	31.01	27.28	760
16	Pr_4N^+	Et_4N^+	35.53	35.53	29.35	1073
17	Bu_4N^+	Pr_4N^+	40.02	40.02	31.35	1459
18	$C_6H_5CH_3$	C_6H_6	30.04	28.59	26.08	630
19	C_6H_5OH	C_6H_6	29.93	29.03	24.30	595
20	$C_6H_5NH_2$	C_6H_6	29.95	28.59	24.84	592

Table II.

(a) Bond Length Parameters

bond	K_r[a]	r_{eq}[b]	bond	K_r[a]	r_{eq}[b]
CT-CT	310	1.526	CA-N2	481	1.340
CT-NT	307	1.492	CA-OH	386	1.364
CT-N2	337	1.460	CA-HC	340	1.083
CT-HC	331	1.090	NT-H	434	1.001
CA-CA	469	1.396	N2-H	434	1.010
CA-CT	317	1.510	OH-HO	553	0.956

(b) Bond Angle Parameters

angle	K_θ[c]	θ_{eq}[d]	angle	K_θ[c]	θ_{eq}[d]
CT-CT-CT	40	109.5	CA-CA-OH	80	117.8
CT-CT-HC	35	109.5	CT-NT-CT	70	109.4
NT-CT-HC	35	109.5	CT-NT-H	35	109.4
N2-CT-HC	35	110.9	H-NT-H	35	113.1
HC-CT-HC	35	109.5	CT-N2-CT	50	109.7
CA-CA-CA	85	120.0	CT-N2-H	38	110.3
CA-CA-CT	70	120.0	CA-N2-H	35	110.3
CA-CA-HC	35	120.0	H-N2-H	35	108.8
CA-CA-N2	70	120.0	CA-OH-HO	55	109.0

[a] In kcal/mol A^2. [b] In Å. [c] In kcal/mol rad^2. [d] In deg. The atom type names used in Tables II and III have the following definitions: CT is sp^3 carbon with four explicit substituents, CA is sp^2 aromatic carbon in a six-membered ring with one substituent, NT is sp^3 nitrogen with four substituents, N2 is sp^2 nitrogen with three substituents, OH is hydroxyl oxygen, H is hydrogen attached to NT or N2, HC is hydrogen attached to CA or CT, and HO is hydrogen attached to OH.

Table III. Nonbonded Interaction Parameters

atom	R (Å)	e (kcal)	atom	R (Å)	ϵ (kcal)
HW[a]	1.000	0.020	N2	1.750	0.160
OH[a]	1.768	0.152	OH	1.650	0.150
CT	1.800	0.060	H	1.000	0.020
CA	1.800	0.060	HC	1.540	0.010
NT	1.850	0.120	HO	1.000	0.020

[a] The atom types HW and OW correspond to hydrogen and oxygen of water, respectively, and the nonbonded parameters of these atoms are used only for solute–solvent interactions. The hydrogen of TIP3P water has a zero van der Waals radius.

x, y, or z direction. The size of the box and the number of water molecules solvating the solute are listed in Table I for each simulation. The force field parameters were assigned for the bonds, angles, and dihedrals of the molecule by the PARM module, which also generates the coordinates file and topology file necessary for the GIBBS module.

The force field parameters for bond lengths and bond angles of the molecules used in the present simulations are listed in Table II(a) and (b). The dihedral parameters are the same as those of Weiner et al.[37]

Table IV. Charges on the Atoms of Normal Alkanes

atom	Me	Et	Pr	Bu
C1	−0.468	−0.187	−0.314	−0.367
H1	0.117	0.062	0.066	0.078
C2		−0.187	0.362	0.197
H2		0.062	−0.064	−0.032
C3			−0.314	0.197
H3			0.066	−0.032
C4				−0.367
H4				0.078

Table V. Charges on the Atoms of Tetraalkylmethane Molecules

atom	Me_4C	Et_4C	Pr_4C	Bu_4C
C	0.143	−0.143	−0.071	−0.068
C1	−0.319	0.130	−0.191	−0.193
H1	0.094	−0.016	0.061	0.075
C2		−0.319	0.129	−0.236
H2		0.085	0.046	0.147
C3			−0.431	0.037
H3			0.101	0.025
C4				−0.281
H4				0.065

Table VI. Charges on the Atoms of Ammonia and Amines

atom	NH_3	$MeNH_2$	Me_2NH	Me_3N
		Electrostatic Potential Charges		
N	−1.076	−0.904	−0.703	−0.379
H	0.359	0.354	0.316	
C1		0.097	0.257	0.092
H1		0.033	−0.021	0.012
		Mulliken Charges		
N	−0.903	−0.870	−0.693	−0.535
H	0.301	0.343	0.339	
C1		−0.278	−0.286	−0.286
H1		0.155	0.154	0.155

The van der Waals parameters, R and e, for TIP3P water and all the solute molecules are listed in Table III. The partial charges were calculated[38] from the electrostatic potential around a molecule obtained with the ab initio program, QUEST[39] using a 6-31G* basis set.[40] For neutral molecules, the charges were uniformly scaled down by a factor of 0.87 to correct the overestimation of dipole moment by 6-31G* basis set. In order to avoid the disk space problem encountered during the ab initio calculations for the largest molecules, Pr_4N^+, Bu_4N^+, Pr_4C, and Bu_4C, we extrapolated the calculated partial charges of the corresponding lower homologues in the following way: the changes on the atoms of propyl groups of $Pr_2N^+Et_2$ were assigned to the atoms of the four propyl groups of Pr_4N^+. In the same way, the calculated charges of $Bu_2N^+Et_2$, Pr_2CEt_2, and Bu_2CEt_2, were used for Bu_4N^+, Pr_4C, and Bu_4C, respectively. For neutral amines, we also performed calculations with Mulliken charges for comparison. The actual partial charges employed for all molecules are listed in Tables IV–VIII.

Before starting the perturbation run using the GIBBS module of the program, each system was minimized by conjugate gradient method by using the BORN module in three stages. First, only the solvent was minimized with periodic boundary conditions for a maximum of 800 cycles, then the whole system was minimized for another 800 cycles, and finally the whole system was minimized using SHAKE for 100 cycles. SHAKE is an algorithm[41] used to constrain the bond lengths to equilibrium values. The system was initially equilibrated for 6.5 ps at constant temperature (300 K) and pressure (1 atm). A time step of 0.002 ps was used for all simulations. During the equilibration and the subsequent perturbation runs the periodic boundary conditions were applied only for solute–solvent and solvent–solvent interactions. The SHAKE procedure was also used during the simulation runs. A cut-off distance of 8 Å was used for solute–solvent and solvent–solvent nonbonded interactions, and

(37) Weiner, S. J.; Kollman, P. A.; Case, D. A.; Singh, U. C.; Ghio, C.; Alagona, G.; Profeta, S.; Weiner, P. *J. Am. Chem. Soc.* **1984**, *106*, 765.
(38) Singh, U. C.; Kollman, P. A. *J. Comput. Chem.* **1984**, *5*, 129.
(39) QUEST (Version 1.0), Singh, U. C.; Kollman, P. A. University of California: San Francisco, 1986.
(40) Hariharan, P. C.; Pople, J. A. *Theor. Chim. Acta* **1973**, *28*, 213.
(41) Ryckaert, J. P.; Ciccotti, G.; Berendsen, H. J. C. *J. Comput. Phys.* **1977**, *23*, 327.

Table VII. Charges on the Atoms of Alkyl- and Tetraalkylammonium Ions

atom	NH_4^+	$MeNH_3^+$	$Me_2NH_2^+$	Me_3NH^+	Me_4N^+	Et_4N^+	Pr_4N^+	Bu_4N^+
N	−0.896	−0.591	−0.045	0.117	0.287	0.287	0.287	0.287
H	0.474	0.404	0.302	0.335				
C1		−0.142	−0.252	−0.380	−0.047	−0.077	−0.397	−0.432
H1		0.174	0.157	0.188	0.216	0.092	0.174	0.193
C2						−0.225	0.201	−0.083
H2						0.099	0.031	0.110
C3							−0.381	0.068
H3							0.115	0.038
C4								−0.371
H4								0.105

Table VIII. Charges on the Atoms of Aromatic Compounds

atom	C_6H_6	$C_6H_5CH_3$	C_6H_5OH	$C_6H_5NH_2$
C1	0.120	−0.363	0.462	0.483
H1	0.120			
C2	0.120	−0.327	−0.298	−0.338
H2	0.120	0.173	0.170	0.168
C3	0.120	−0.087	−0.060	−0.066
H3	0.120	0.140	0.127	0.128
C4	0.120	−0.222	−0.230	−0.209
H4	0.120	0.153	0.135	0.131
C5	0.120	−0.327	−0.022	−0.066
H5	0.120	0.173	0.124	0.128
C6	0.120	−0.087	−0.389	−0.338
H6	0.120	0.140	0.163	0.168
C		−0.473		
H		0.127		
O			−0.563	
H			0.380	
N				−0.775
H				0.295

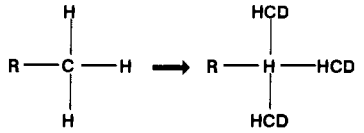

Figure 1. A schematic diagram showing the mapping of one molecule on to another by direct atom-to-atom assignment during mutation of a methyl group of a hydrocarbon. The symbols R, C, H, and HCD represent an alkyl group, a carbon, a hydrogen, and a dummy atom, respectively.

all solute–solute nonbonded interactions were included. A constant dielectric ($\epsilon = 1$) was used for all simulations. Mutation was achieved by mapping one molecule onto the other by direct atom-to-atom assignment. A typical case where a methyl group is mutated to a hydrogen atom is schematically shown in Figure 1. The atoms C and H in the initial state of the molecule are transformed to atoms H and HCD, respectively, by mutating the respective partial charges and van der Waals parameters. The dummy atom, HCD, carries no partial charge, and the angle R–HC–HCD remains the same as R–CT–HC. As stated in the earlier section, the transformation was achieved in two stages. In the first run, the charges were mutated and the van der Waals parameters in the second run; thus the two contributions to free energy change were calculated separately. In all cases, the "window method" was employed. For the electrostatic run, 21 windows were used, and at each window the system was equilibrated for 1.0 ps, and the data were collected over the next 1.0 ps. The van der Waals parameters were mutated with and without coordinate coupling in most of the cases. Simulations without the coordinate coupling were divided into 101 windows with equilibration for 0.4 ps and data collection for the next 0.4 ps at each window. With the coordinate coupling, the simulations were divided into 201 windows with 0.2 ps of equilibration and 0.2 ps of data collection. For a few simulations, the time span for the van der Waals run was doubled (with 201 windows and 0.4 ps of equilibration and 0.4 ps of data collection at each window) to check the dependence of calculated values on the length of simulation time. In all cases, the difference between the values calculated in the two runs was within the expected fluctuations (<4%).

Results

The various contributions to the calculated free energy changes and their sums for different transformations are summarized in Table IX. For each simulation, the electrostatic contribution, ΔG_{ele}, and the van der Waals contribution with coordinate coupling, $\Delta G_{vdw/cc}$, and their sum are listed. Except for a few simulations, the van der Waals contribution without the coordinate coupling, ΔG_{vdw}, was also calculated, and these values along with their sums with ΔG_{ele} are also listed. The reported ΔG_{ele}, $\Delta G_{vdw/cc}$, and ΔG_{vdw} values are the averages of the values obtained from the forward and the backward simulations. The experimental values available in the literature[42-46] are listed for comparison in the last column of Table IX.

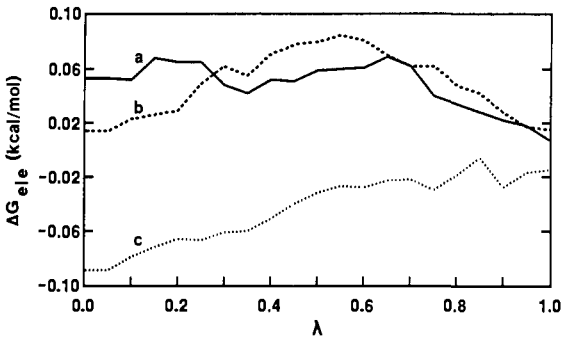

Figure 2. Variation of ΔG_{ele} with λ for normal alkanes: (a) $C_4H_{10} \rightarrow C_3H_8$, (b) $C_3H_8 \rightarrow C_2H_6$, and (c) $C_2H_6 \rightarrow CH_4$.

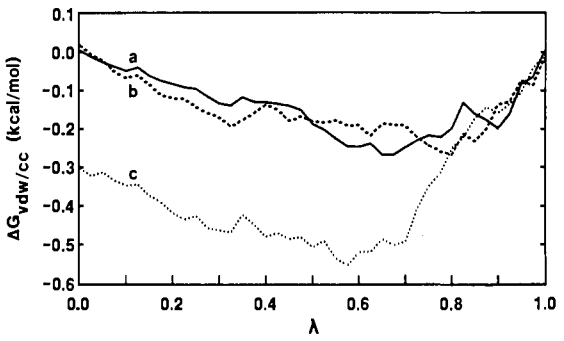

Figure 3. Variation of $\Delta G_{vdw/cc}$ with λ for normal alkanes: (a) $C_4H_{10} \rightarrow C_3H_8$, (b) $C_3H_8 \rightarrow C_2H_6$, and (c) $C_2H_6 \rightarrow CH_4$.

Simulations 1, 2, and 3 correspond to the transformations of simple alkanes, namely, $C_2H_6 \rightarrow CH_4$, $C_3H_8 \rightarrow C_2H_6$, and $C_4H_{10} \rightarrow C_3H_8$, respectively. The respective ΔG_{ele} values for these simulations are −0.09, 0.01, and 0.05 kcal/mol, and the $\Delta G_{vdw/cc}$ values are −0.33, 0.02, and 0.01 kcal/mol. The corresponding total free energy changes are −0.42, 0.03, and 0.06 kcal/mol. The ΔG_{vdw} values for these simulations are 0.14, 0.09, and 0.18 kcal/mol, respectively, and the corresponding total free energies are 0.05, 0.10, and 0.23 kcal/mol. The total free energies obtained with and without the coordinate coupling do not quite agree with

(42) Wilhelm, E.; Battino, R.; Wilcock, R. J. *Chem. Rev.* **1977**, *77*, 219.
(43) Abraham, M. H. *J. Am. Chem. Soc.* **1982**, *104*, 2085.
(44) (a) Jones, F. M.; Arnett, E. M. *Prog. Phys. Org. Chem.* **1974**, *11*, 263. (b) Arnett, E. M.; Jones, III, F. M.; Taagepera, M.; Henderson, W. G.; Beauchamp, J. L.; Holtz, D.; Taft, R. W. *J. Am. Chem. Soc.* **1972**, *94*, 4724.
(45) Abraham, M. H.; Liszi, J. *J. Chem. Soc., Faraday Trans. 1* **1978**, *74*, 1604.
(46) Seidell, A. *Solubilities of Organic Compounds*, 3rd ed.; Van Nostrand: New York, 1941; Vol. 2.

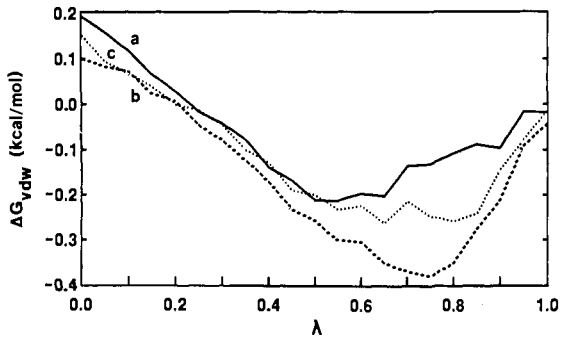

Figure 4. Variation of ΔG_{vdw} with λ for normal alkanes: (a) $C_4H_{10} \rightarrow C_3H_8$, (b) $C_3H_8 \rightarrow C_2H_6$, and (c) $C_2H_6 \rightarrow CH_4$.

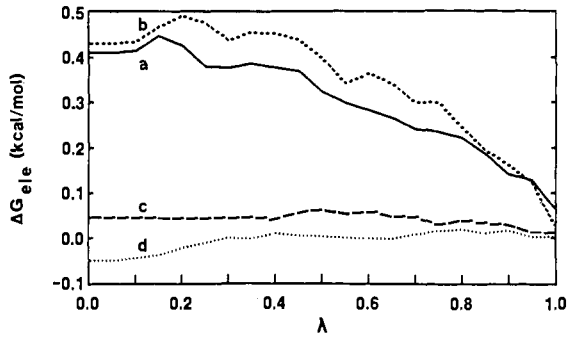

Figure 5. Variation of ΔG_{ele} with λ for symmetrical tetraalkylmethane molecules: (a) $Bu_4C \rightarrow Pr_4C$, (b) $Pr_4C \rightarrow Et_4C$, (c) $Et_4C \rightarrow Me_4C$, and (d) $Me_4C \rightarrow CH_4$.

the experimental values of 0.17, −0.12, and −0.12 kcal/mol. The variations of ΔG_{elc}, $\Delta G_{vdw/cc}$, and ΔG_{vdw} with λ are shown in Figures 2, 3, and 4, respectively. For simulation 1, ΔG_{elc} decreases almost linearly to −0.09 kcal/mol, whereas for simulation 2, it initially increases and then decreases to 0.01 kcal/mol. For simulation 3, it shows a steadier increase to a value of 0.05 kcal/mol. For all simulations, $\Delta G_{vdw/cc}$ initially decreases and then increases with λ. Although the initial decrease is much larger in simulation 1 than in the other simulations, the rise after the dip is almost parallel. ΔG_{vdw} behaves similarly in all three cases, with an initial decrease and then an increase to reach about the same final value.

Simulations 4, 5, 6, and 7 correspond to transformations of symmetrical tetraalkylmethane molecules, namely, $Me_4C \rightarrow CH_4$, $Et_4C \rightarrow Me_4C$, $Pr_4C \rightarrow Et_4C$, and $Bu_4C \rightarrow Pr_4C$, respectively. Since four methyl groups are mutated to four hydrogens in these simulations, the degree of perturbation is 4-fold larger than for alkanes. Therefore, larger free energy changes are expected for these simulations. The ΔG_{ele} values for the simulations 4, 5, 6, and 7 are −0.05, 0.05, 0.44, and 0.41 kcal/mol, respectively. The first two values are comparable to the ΔG_{ele} values of simple alkanes, whereas the latter two values are higher. The respective $\Delta G_{vdw/cc}$ values for these simulations are −0.81, 0.35, −1.03, and −0.92 kcal/mol, and the total free energy changes are −0.86, 0.40, −0.59, and −0.51 kcal/mol. The total free energy changes (−0.86 and 0.40 kcal/mol) for simulations 4 and 5 compare well with the available experimental values of −0.50 and 0.28 kcal/mol. The van der Waals contributions obtained without coordinate coupling, ΔG_{vdw}, for simulations 4 and 5 are 1.34 and 0.81 kcal/mol, respectively, and the corresponding total free energy changes are 1.29 and 0.86 kcal/mol. These values are not as close to the experimental values as those obtained with the coordinate coupling. As shown in Figure 5, the plots of ΔG_{ele} vs λ shows that ΔG_{ele} decreases for simulation 4, remains almost constant for simulation 5, and increases for simulations 6 and 7. From the plots of $\Delta G_{vdw/cc}$ vs λ (Figure 6), it may be noted that $\Delta G_{vdw/cc}$ shows a dip which is similar to that observed for alkanes (Figure 3). The initial decrease is most pronounced for simulation 6 and is small for simulation 5. $\Delta G_{vdw/cc}$ reaches about −1.0 kcal/mol for simulations 4, 6, and 7. Qualitatively the same trend can be seen from the

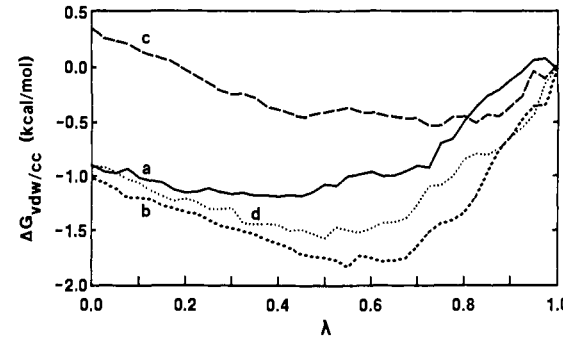

Figure 6. Variation of $\Delta G_{vdw/cc}$ with λ for symmetrical tetraalkylmethane molecules: (a) $Bu_4C \rightarrow Pr_4C$, (b) $Pr_4C \rightarrow Et_4C$, (c) $Et_4C \rightarrow Me_4C$, and (d) $Me_4C \rightarrow CH_4$.

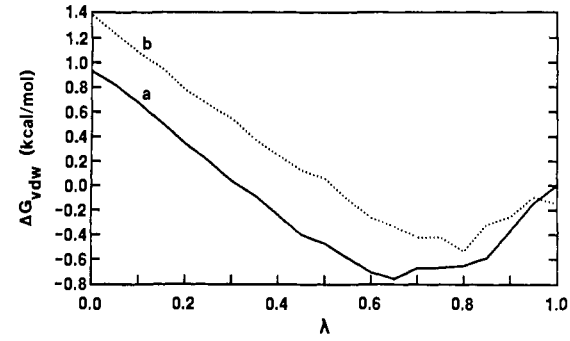

Figure 7. Variation of ΔG_{vdw} with λ for symmetrical tetraalkylmethane molecules: (a) $Et_4C \rightarrow Me_4C$ and (b) $Me_4C \rightarrow CH_4$.

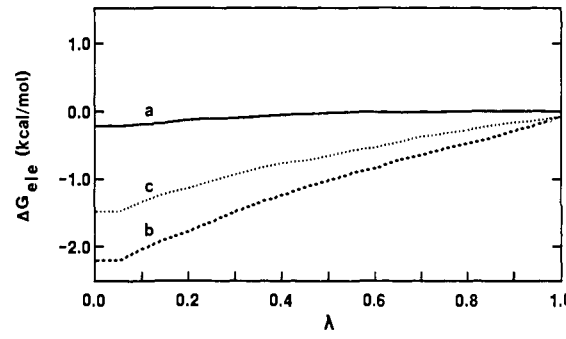

Figure 8. Variation of ΔG_{ele} with λ for neutral amines: (a) $MeNH_2 \rightarrow NH_3$, (b) $Me_2NH \rightarrow MeNH_2$, and (c) $Me_3N \rightarrow Me_2NH$.

plots of ΔG_{vdw} vs λ, shown in Figure 7, for simulations 4 and 5. However, the rise after the dip in $\Delta G_{vdw/cc}$ variation is smaller than that observed in ΔG_{vdw} variation. Similar behavior was also noted for normal alkanes.

Simulations 8, 9, and 10 represent transformations between primary, secondary, and tertiary neutral amines, $MeNH_2 \rightarrow NH_3$, $Me_2NH \rightarrow MeNH_2$, and $Me_3N \rightarrow Me_2NH$, respectively. The respective ΔG_{ele} values for these simulations are −0.21, −2.21, and −1.47 kcal/mol, and the $\Delta G_{vdw/cc}$ values are 0.28, 0.28, and 0.30 kcal/mol. The corresponding total free energy changes are 0.07, −1.93, and −1.17 kcal/mol, which are of the same order as the experimental values (Table IX). For simulation 10, the calculated value (−1.17 kcal/mol) is very close to the experimental value (−1.07 kcal/mol). For simulation 8, the discrepancy between the calculated value (0.07 kcal/mol) and the experimental value (0.27 kcal/mol) stems from a large hysteresis in the van der Waals contribution. The discrepancy between the calculated value (−1.93 kcal/mol) and the experimental value (−0.27 kcal/mol) comes from the electrostatic contribution for simulation 9. In all cases, ΔG_{ele} decreases linearly with λ as shown in Figure 8, and the decrease is highest for simulation 9. In contrast, $\Delta G_{vdw/cc}$ increases in the same zigzag pattern for all these simulations (Figure 9).

Calculations for the three transformations of amines were repeated with Mulliken charges to study the effect of different partial

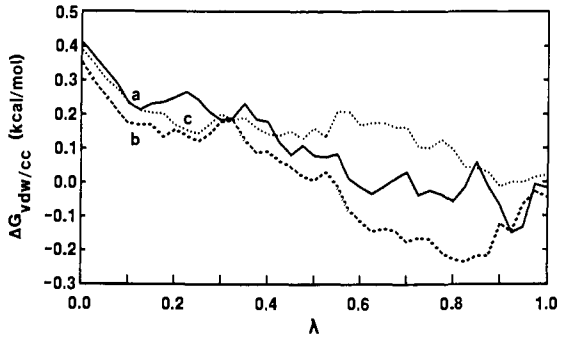

Figure 9. Variation of $\Delta G_{vdw/cc}$ with λ for neutral amines: (a) $MeNH_2 \rightarrow NH_3$, (b) $Me_2NH \rightarrow MeNH_2$, and (c) $Me_3N \rightarrow Me_2NH$.

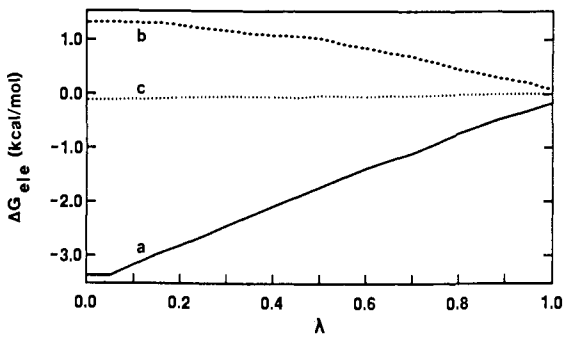

Figure 10. Variation of ΔG_{ele} with λ for alkyl ammonium ions: (a) $MeNH_3^+ \rightarrow NH_4^+$, (b) $Me_2NH_2^+ \rightarrow MeNH_3^+$, and (c) $Me_3NH^+ \rightarrow Me_2NH_2^+$.

charge distributions on the calculated free energy changes. The new ΔG_{ele} values for simulations 8, 9, and 10 are 1.10, −0.32, and −0.10 kcal/mol, respectively, and the $\Delta G_{vdw/cc}$ values are 0.10, 0.19, and 0.45 kcal/mol, respectively. The corresponding total free energy changes are 1.20, −0.13, and 0.35 kcal/mol, which are in greater discrepancy with the experimental values than the results of earlier simulations. Even the signs are not in the correct order. The discrepancy seems to stem from the ΔG_{ele} values which differ greatly from the ΔG_{ele} values of earlier simulations. The $\Delta G_{vdw/cc}$ values do not differ much in the two cases. These comparative simulations show that the calculated free energies depend on the partial charges of the solute molecule, particularly when the electrostatic contribution to free energy dominates.

Transformations involving primary, secondary, and tertiary alkylammonium ions, $MeNH_3^+ \rightarrow NH_4^+$, $Me_2NH_2^+ \rightarrow MeNH_3^+$, and $Me_3NH^+ \rightarrow Me_2NH_2^+$, are represented by simulations 11, 12, and 13, respectively. The respective ΔG_{ele} values for these simulations are −3.35, 1.36, and −0.11 kcal/mol, and the $\Delta G_{vdw/cc}$ values are −5.73, −7.71, and −5.76 kcal/mol. The corresponding total free energy values, −9.08, −6.35, and −5.87 kcal/mol, are in good agreement with the experimental values of −7.30, −6.40, and −7.00 kcal/mol, respectively. Only for simulation 11, the van der Waals run was performed without the coordinate coupling, and the corresponding free energy value, −9.64 kcal/mol, is quite close to the value (−9.08 kcal/mol) obtained with the coordinate coupling. As shown in Figure 10, ΔG_{ele} decreases linearly for simulation 11, increases linearly for simulation 12, and remains almost constant for simulation 13. However, $\Delta G_{vdw/cc}$ decreases uniformly in all cases (Figure 11).

Simulations 14, 15, 16, and 17 represent the transformations of tetraalkylammonium ions, i.e., $Me_4N^+ \rightarrow NH_4^+$, $Et_4N^+ \rightarrow Me_4N^+$, $Pr_4N^+ \rightarrow Et_4N^+$, and $Bu_4N^+ \rightarrow Pr_4N^+$. For these simulations, the ΔG_{ele} values are −0.65, −0.64, −1.33, and 0.35 kcal/mol, respectively, and the $\Delta G_{vdw/cc}$ values are −29.17, −6.10, −4.26, and −3.10, kcal/mol, respectively. The corresponding total free energy changes are −29.82, −6.74, −5.59, and −2.75 kcal/mol. The respective ΔG_{vdw} values are −23.64, −2.92, −1.25, and −0.64 kcal/mol, and the corresponding total free energy changes are −24.28, −3.54, −2.58, and −0.29 kcal/mol. The experimental values available for simulations 16 and 17 are −31.70 and −7.00 kcal/mol,

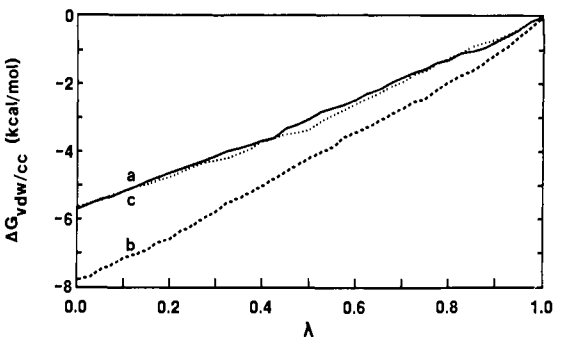

Figure 11. Variation of $\Delta G_{vdw/cc}$ with λ for alkyl ammonium ions: (a) $MeNH_3^+ \rightarrow NH_4^+$, (b) $Me_2NH_2^+ \rightarrow MeNH_3^+$, and (c) $Me_3NH^+ \rightarrow Me_2NH_2^+$.

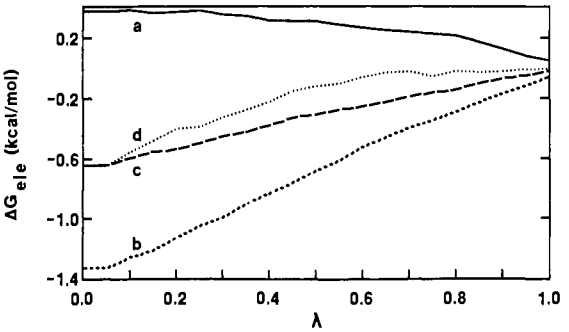

Figure 12. Variation of ΔG_{ele} with λ for symmetrical tetraalkylammonium ions: (a) $Bu_4N^+ \rightarrow Pr_4N^+$, (b) $Pr_4N^+ \rightarrow Et_4N^+$, (c) $Et_4N^+ \rightarrow Me_4N^+$, and (d) $Me_4N^+ \rightarrow NH_4^+$.

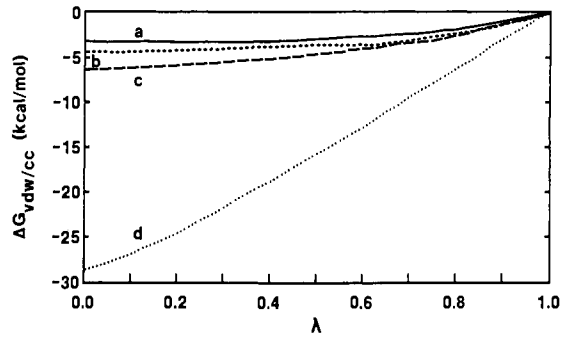

Figure 13. Variation of $\Delta G_{vdw/cc}$ with λ for symmetrical tetraalkylammonium ions: (a) $Bu_4N^+ \rightarrow Pr_4N^+$, (b) $Pr_4N^+ \rightarrow Et_4N^+$, (c) $Et_4N^+ \rightarrow Me_4N^+$, and (d) $Me_4N^+ \rightarrow NH_4^+$.

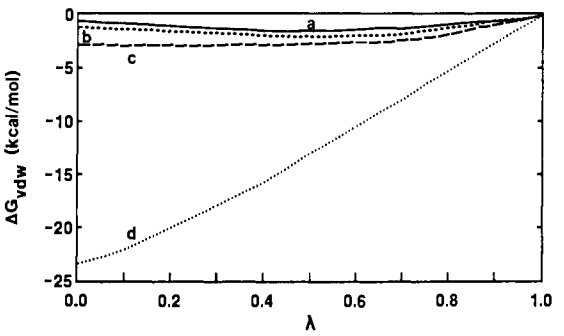

Figure 14. Variation of ΔG_{vdw} for λ for symmetrical tetraalkylammonium ions: (a) $Bu_4N^+ \rightarrow Pr_4N^+$, (b) $Pr_4N^+ \rightarrow Et_4N^+$, (c) $Et_4N^+ \rightarrow Me_4N^+$, and (d) $Me_4N^+ \rightarrow NH_4^+$.

respectively, which are closer to the calculated values obtained with the coordinate coupling. The plots for ΔG_{ele}, $\Delta G_{vdw/cc}$, and ΔG_{vdw} vs λ are given in Figures 12, 13, , and 14, respectively. The electrostatic contribution, ΔG_{ele}, decreases almost linearly in all cases except simulation 17, which shows an increasing trend. The van der Waals contribution with or without coordinate coupling

Table IX. Calculated and Experimental Free Energy Changes[f]

solute	ref	ΔG_{ele}	$\Delta G_{vdw/cc}$	total	expt
C_2H_6	CH_4	−0.09 ± 0.01	−0.33 ± 0.02	−0.42 ± 0.03	0.17[a]
†			0.14 ± 0.01	0.05 ± 0.02	
C_3H_8	C_2H_6	0.01 ± 0.00	0.02 ± 0.01	0.03 ± 0.01	−0.12[a]
†			0.09 ± 0.01	0.10 ± 0.01	
C_4H_{10}	C_3H_8	0.05 ± 0.00	0.01 ± 0.00	0.06 ± 0.01	−0.12[a]
†			0.18 ± 0.01	0.23 ± 0.01	
Me_4C	CH_4	−0.05 ± 0.01	−0.81 ± 0.07	−0.86 ± 0.08	−0.50[b]
†			1.34 ± 0.04	1.29 ± 0.05	
Et_4C	Me_4C	0.05 ± 0.00	0.35 ± 0.01	0.40 ± 0.01	0.28[b]
†			0.81 ± 0.11	0.86 ± 0.11	
Pr_4C	Et_4C	0.44 ± 0.01	−1.03 ± 0.01	−0.59 ± 0.02	
Bu_4C	Pr_4C	0.41 ± 0.01	−0.92 ± 0.02	−0.51 ± 0.03	
$MeNH_2$	NH_3	−0.21 ± 0.00	0.28 ± 0.13	0.07 ± 0.13	0.27[c]
‡		1.10 ± 0.01	0.10 ± 0.08	1.20 ± 0.09	
Me_2NH	$MeNH_2$	−2.21 ± 0.01	0.28 ± 0.07	−1.93 ± 0.08	−0.27[c]
‡		−0.32 ± 0.00	0.19 ± 0.12	−0.13 ± 0.12	
Me_3N	Me_2NH	−1.47 ± 0.01	0.30 ± 0.05	−1.17 ± 0.06	−1.07[c]
‡		−0.10 ± 0.00	0.45 ± 0.12	0.35 ± 0.12	
$MeNH_3^+$	NH_4^+	−3.35 ± 0.02	−5.73 ± 0.10	−9.08 ± 0.12	−7.30[c]
†			−6.29 ± 0.04	−9.64 ± 0.06	
$Me_2NH_2^+$	$MeNH_3^+$	1.36 ± 0.04	−7.71 ± 0.09	−6.35 ± 0.13	−6.40[c]
Me_3NH^+	$Me_2NH_2^+$	−0.11 ± 0.00	−5.76 ± 0.05	−5.87 ± 0.05	−7.00[c]
Me_4N^+	NH_{4+}	−0.65 ± 0.00	−29.17 ± 0.52	−29.82 ± 0.52	−31.70[c]
†			−23.64 ± 0.24	−24.28 ± 0.24	
Et_4N^+	Me_4N^+	−0.64 ± 0.01	−6.10 ± 0.25	−6.74 ± 0.26	−7.00[d]
†			−2.92 ± 0.09	−3.54 ± 0.10	
Pr_4N^+	Et_4N^+	−1.33 ± 0.01	−4.26 ± 0.10	−5.59 ± 0.11	
†			−1.25 ± 0.05	−2.58 ± 0.06	
Bu_4N^+	Pr_4N^+	0.35 ± 0.02	−3.10 ± 0.06	−2.75 ± 0.08	
†			−0.64 ± 0.01	−0.29 ± 0.03	
$C_6H_5CH_3$	C_6H_6	−0.32 ± 0.01	−0.10 ± 0.02	−0.42 ± 0.03	−0.86[e]
†			0.38 ± 0.02	0.06 ± 0.03	
C_6H_5OH	C_6H_6	2.52 ± 0.01	1.00 ± 0.00	3.52 ± 0.01	2.20[e]
$C_6H_5NH_2$	C_6H_6	1.05 ± 0.01	1.16 ± 0.01	2.21 ± 0.02	1.68[e]
†			1.24 ± 0.01	2.29 ± 0.02	

[a–e] For a, b, c, d, and e see ref 42–46, respectively. [f] All values are in kcal/mol, † without coordinate coupling, ‡ with Mulliken charges.

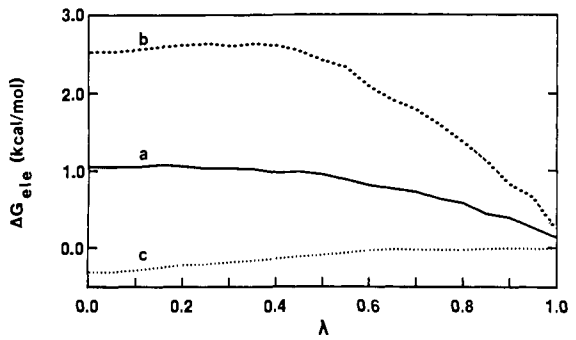

Figure 15. Variation of ΔG_{ele} with λ for aromatic compounds: (a) aniline → benzene, (b) phenol → benzene, and (c) toluene → benzene.

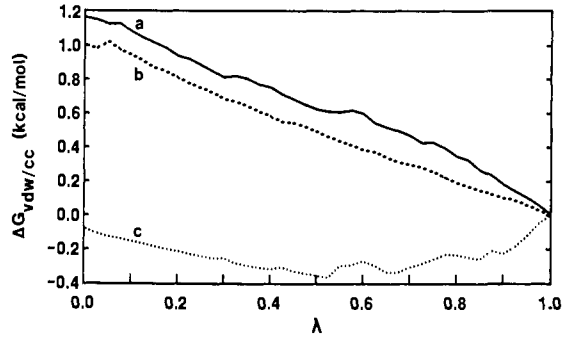

Figure 16. Variation of $\Delta G_{vdw/cc}$ with λ for aromatic compounds: (a) aniline → benzene, (b) phenol → benzene, and (c) toluene → benzene.

decreases initially and then flattens in simulations 14, 15, and 16, whereas it decreases continuously with a large slope for simulation 17.

Transformations of aromatic compounds, toluene → benzene, phenol → benzene, and aniline → benzene are represented by simulations 18, 19, and 20, respectively. The respective ΔG_{ele} values for these simulations are −0.32, 2.52, and 1.05 kcal/mol, and the $\Delta G_{vdw/cc}$ values are −0.10, 1.00, and 1.16 kcal/mol. The corresponding total free energy changes are −0.42, 3.52, and 2.21 kcal/mol, which are in reasonable agreement with the experimental values of −0.86, 2.20, and 1.68 kcal/mol. The ΔG_{vdw} values obtained for simulations 18 and 20 are 0.38 and 1.24, respectively. The corresponding total free energy changes, 0.06 and 2.29 kcal/mol, are in poor agreement with the experimental values. The plots of the variation of ΔG_{ele} and $\Delta G_{vdw/cc}$ vs λ are shown in Figures 15 and 16, respectively. ΔG_{ele} initially increases and then flattens in simulations 19 and 20, whereas it decreases almost linearly in simulation 18. $\Delta G_{vdw/cc}$ shows a linear increase for simulations 19 and 20, whereas it initially decreases and then increases in simulation 18. It may be noted that the pattern of variation of $\Delta G_{vdw/cc}$ with λ for toluene → benzene transformation (simulation 18) tends to resemble that of hydrophobic alkanes, whereas the patterns for phenol → benzene and aniline → benzene transformation (simulations 19 and 20) resemble those of amines.

Discussion

The calculated free energy changes for the transformations studied here agree reasonably well with the experimental values in all cases except for normal alkanes. In particular, the total free energy changes obtained with the coordinate coupling are closer to the experimental values than those obtained without the coordinate coupling. This clearly results from resetting the coordinates of the disappearing groups for the $\lambda_{i\pm1}$ windows while calculating the interaction energies with the coordinate coupling approach. The discrepancy between calculated and experimental values of normal alkanes may be due to the following three factors. First, the expected free energy changes are too small (of the order of 0.15 kcal/mol) and are comparable to the fluctuations in calculated values. Second, the solvent around the solute undergoes an unsymmetrical reorganization during the mutation of normal

Table X. Interaction Energies and Experimental Heats of Hydration[f]

solute	interaction energy	rms deviation	ΔH
CH_4	-2.8	0.6	-3.3[a]
C_2H_6	-4.9	0.7	-4.7[a]
C_3H_8	-5.7	0.7	-5.4[a]
C_4H_{10}	-7.0	1.0	-6.2[a]
Me_4C	-8.4	0.8	-6.6[b]
Et_4C	-13.2	0.9	-9.8[b]
Pr_4C	-18.9	1.2	
Bu_4C	-24.7	1.4	
NH_3	-7.5	0.9	-8.4[c]
$MeNH_2$	-15.0	2.1	-10.8[c]
Me_2NH	-18.1	1.6	-13.3[c]
Me_3N	-17.0	2.2	-13.2[c]
NH_4^+	-138.5	6.4	-84.0[c]
$MeNH_3^+$	-117.8	7.0	-75.4[c]
$Me_2NH_2^+$	-111.4	5.7	-69.7[c]
Me_3NH^+	-101.6	5.7	-63.3[c]
Me_4N^+	-100.2	7.0	-51.9[d]
Et_4N^+	-96.7	5.9	-42.1[d]
Pr_4N^+	-97.3	7.2	-48.0[d]
Bu_4N^+	-96.5	5.0	
C_6H_6	-17.6	1.5	-8.7[e]
$C_6H_5CH_3$	-16.2	1.8	-7.3[e]
C_6H_5OH	-23.9	3.7	
$C_6H_5NH_2$	-20.0	2.0	

[a-e] For a, b, c, d, and e see ref 42, 43, 44, 47, and 48, respectively.

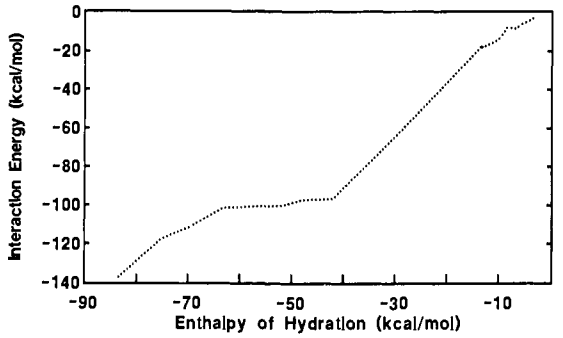

Figure 17. Plot of the calculated interaction energies vs the experimental heats of hydration for various solutes.

alkanes. For instance, during the conversion of ethane → methane, the solvent shell around the solute changes in shape from a peanut to a ball, which may require large change in the solvent structure. To circumvent this situation, we repeated these simulations with longer periods (250 ps) of equilibration and data collection, but the discrepancy still persisted. Third, the interaction energies (listed in Table X and discussed in the next paragraph) for alkanes are smaller than the other molecules; hence, the inherent uncertainties in calculated free energies for alkanes may be larger than those for molecules with larger interaction energies.

To find out whether the free energy change for different transformations is dominated by entropic or enthalpic contributions, the calculated solute–solvent interaction energies are examined and compared with the experimental heats of hydration (ΔH) reported in the literature.[42-48] These values are given in Table X. For simple alkanes, the interaction energies are very close to the ΔH values, whereas for larger molecules the interaction energies are much larger. The plot of interaction energy versus ΔH, given in Figure 17, may be divided into several regions which represent a different class of compounds examined here, and, in each region, the interaction energy varies almost linearly with ΔH. The interaction energies of hydrophobic normal alkanes and tetraalkylmethane molecules decrease with the decreasing size of the molecule. This decrease is about 1.2 kcal/mol per methyl group as compared to a decrease of about 0.8 kcal/mol per methyl group in ΔH. The interaction energies for amines are about 1.5 times ΔH and show an irregular pattern similar to that of ΔH. For alkyl-substituted and tetraalkyl-substituted ammonium ions, the interaction energies are as large as about 1.5–2.0 times ΔH. Unlike neutral hydrophobic molecules, the interaction energies for these ions show a marginal increase with the decreasing size of the molecule. This is not surprising since the charge density per Å^2 at the surface of the ions bearing large hydrocarbon groups is larger for smaller molecules, and, as a result, these ions interact more strongly with water. Therefore, enthalpy change favors transformation of a higher homologue to a lower homologue in these cases but does not favor a similar transformation of simple hydrocarbons and tetraalkylmethane molecules. For aromatic compounds, the interaction energies are almost twice the experimental ΔH, and the former values are comparable for toluene and benzene whereas those of phenol and aniline are higher. This is expected since the dipole moments[49] of phenol (1.45 debye) and aniline (1.53 debye) are very much larger than those of toluene (0.36 debye) and benzene (0 debye). Therefore, phenol and aniline interact more strongly with water than toluene or benzene, and, hence, enthalpy change does not favor phenol → benzene and aniline → benzene transformations.

Further insight into the differences in the hydration processes of different solutes is obtained by examining the variation of free energy change with λ. The free energy variation with the mutation of partial charges of a solute does not conform to any regular pattern, since it is dictated by the partial charge distributions of the initial and final states of the solute molecule. However, the free energy variations with mutation of van der Waals parameters for transformations within a series of the same class of compounds show definite trends. The differences in these trends and their implications for the process of hydration are discussed in the following paragraphs for each series of transformations.

Tetraalkylammonium ions are taken as model hydrophobic systems for many experimental studies. Therefore, we discuss first the results of the simulations of these ions. The van der Waals contribution to free energy calculated with and without coordinate coupling decreases almost linearly with λ for the $Me_4N^+ \rightarrow NH_4^+$ transformation, whereas it decreases linearly up to $\lambda = 0.8$ and then becomes almost flat with further decrease in λ for the other three transformations (Figures 13 and 14). This behavior can be explained if we presume that water molecules around the solute are "repulsed" by the hydrophobic methyl groups and form a strongly bound solvation shell around the solute in accordance with Frank and Evans' hypothesis.[4] Because of the unit positive charge on tetraalkylammonium ions, the solvent is strongly pulled toward the solute, which results in a configuration wherein the solute and the surrounding solvent are further pushed into the repulsive region of the solute–solvent nonbonded interaction potential surface. Since the van der Waals interactions from four methyl groups disappear during mutation, the repulsive solute–solvent interaction is relieved, resulting in a decrease in free energy. The continuous decrease in free energy with λ for the $Me_4N^+ \rightarrow NH_4^+$ transformation is, however, magnified by the favorable interaction between NH_4^+ and water through hydrogen bond formation. Thus, the mutation of methyl groups to hydrogens eases the tightly bound water structure causing an increase in entropy,[50] and the enhanced solute–solvent interaction causes a decrease in enthalpy. In fact, the calculated interaction energies decrease from -100.2 to -138.5 kcal/mol when one goes from Me_4N^+ to NH_4^+. Hence, the continuous and steep decrease in free energy is due to both favorable entropic and enthalpic contributions. For three transformations, $Bu_4N^+ \rightarrow Pr_4N^+$, $Pr_4N^+ \rightarrow Et_4N^+$, and $Et_4N^+ \rightarrow Me_4N^+$, disappearance of the four terminal methyl groups does not lead to formation of any hydrogen bonds with the surrounding water. Therefore, no continuous

(47) Boyd, R. H. *J. Chem. Phys.* **1969**, *51*, 1470.
(48) Gill. S. J.; Nichols, N. F.; Wadso, I. *J. Chem. Thermodyn.* **1978**, *74*, 1604.
(49) Weast, R. C. *Handbook of Chemistry and Physics*, 63rd ed.; CRC: FL, 1982–1983; pp E-59–E-61.
(50) The rotational correlation time of water in the vicinity of tetraalkylammonium ions decreases with decreasing size of the ion. See: (a) Endom, L.; Hertz, H. G.; Thul, B.; Zeidler, M. D. *Ber. Bunsenges. Phys. Chem.* **1967**, *71*, 1008. (b) Hertz, H. G.; Zeidler, M. D. *Ber. Bunsenges. Phys. Chem.* **1964**, *68*, 621.

decrease in free energy with λ occurs. Nevertheless, free energy initially decreases up to $\lambda = 0.8$ due to the decrease in the repulsive solute–solvent interaction. At lower values of λ, the solute–solvent configuration is not any more in the repulsive region of the interaction potential surface, since the van der Waals parameters of the disappearing methyl groups are reduced. Hence, any further decrease in van der Waals parameters does not favor a decrease in free energy. Moreover, the calculated interaction energies of the solutes at the beginning and the end of transformation remain almost the same. Therefore, the latter part of the transformation is not favored by the enthalpic contribution as in the $Me_4N^+ \rightarrow NH_4^+$ transformation.

For neutral tetraalkylmethane molecules, the $\Delta G_{vdw/cc}$ component for the transformations $Bu_4C \rightarrow Pr_4C$, $Pr_4C \rightarrow Et_4C$, $Et_4C \rightarrow Me_4C$, and $Me_4C \rightarrow CH_4$ decreases almost linearly as λ goes from 1 → 0.75, remains flat up to $\lambda = 0.4$, and then increases as λ goes from 0.4 → 0.0 (Figure 6). The initial decrease is not as large as in the transformations of tetraalkylammonium ions. The initial dip is at about −1.5 kcal/mol in all cases except the $Pr_4C \rightarrow Et_4C$ transformation, for which the dip is at −0.5 kcal/mol. The initial decrease is consistent with the fact that the solute and solvent are in the repulsive region of the interaction potential energy surface. However, the effect is not as amplified as in tetraalkylammonium ions, which possess a net unit positive charge. Further, the interaction energy of the solute increases during the transformation in this series. In other words, the transformation is endothermic; hence, the free energy increases during the latter part of the transformation. The same is also true for the transformations involving normal alkanes, since the trend in the variation of $\Delta G_{vdw/cc}$ for alkanes (Figure 3) is similar to that observed for tetraalkylmethane molecules. However, the magnitude of variation in free energy is much lower due to much smaller interaction energies (Table X). This picture of hydration seems to support the conclusion, drawn from the analysis of solvation data of apolar solutes by Abraham,[43] that the hydrophobic effect is primarily an enthalpic effect, originating in endothermic $-CH_3$/water interactions.

For alkyl-substituted ammonium ions, $\Delta G_{vdw/cc}$ decreases in all cases (Figure 11) in a manner similar to that observed for the transformation $Me_4N^+ \rightarrow NH_4^+$. Each transformation in this series involves mutation of a methyl group which, in addition to reducing the repulsive solute–water interaction, makes the solute capable of forming an additional hydrogen bond with water. Hence, the transformation is facilitated by favorable enthalpic and entropic contributions. In fact, the interaction energy decreases with the mutation of the solute. Moreover, the $\Delta G_{vdw/cc}$ values for all the transformations in this series are close to around −6.0 to −7.0 kcal/mol. This value is comparable to the quarter of −29.17 kcal/mol, obtained for $Me_4N^+ \rightarrow NH_4^+$ transformation in which four methyl groups are mutated to four hydrogens. This correlation suggests that the free energy contribution from a methyl group is roughly additive for alkyl-substituted ammonium ions.

In the cases discussed so far, the dominant contribution to free energy change comes from the mutation of van der Waals parameters. However, for neutral amines, ΔG_{ele} has dominant contribution to free energy change over the $\Delta G_{vdw/cc}$ contribution. This is expected since amines are polar molecules, which have net dipole moments. Therefore, the free energy change during transformations of amines is mainly dictated by change in the dipole moment of the molecule, which is computed during the electrostatic run. The dipole moments[49] of amines increase from 0.61 → 1.03 → 1.31 → 1.47 as one goes along $Me_3N \rightarrow Me_2NH \rightarrow MeNH_2 \rightarrow NH_3$. This trend is reflected by the ΔG_{ele} values, though this value for the $Me_2NH \rightarrow MeNH_2$ transformation is unexpectedly large. In contrast, the ΔG_{ele} values calculated with Mulliken charges show a trend which is inconsistent with the variation of dipole moments. The $\Delta G_{vdw/cc}$ values are almost the same in all cases and show an almost linear increase in λ (Figure 9) without any prominent dip as in hydrocarbons. This is surprising considering the fact that the interaction energy decreases or remains constant during these transformations. This may be due to the fact that amines are capable of forming directional hydrogen bonds with water, and the structure of the water shell around amines is dictated by these hydrogen bonds. Therefore, it may not be reasonable to expect $\Delta G_{vdw/cc}$ to vary with λ in the same way as in alkanes or alkylammonium ions. Further, it may not be reasonable to deduce a picture of hydration of amines on the basis of the $\Delta G_{vdw/cc}$ variation with λ, since ΔG_{ele} has major contribution to free energy change. On the other hand, hydration process of amines seems to be dictated by dipole moments as reflected in the ΔG_{ele} values.

For aromatic compounds, two different kinds of behavior occur. Both ΔG_{ele} and $\Delta G_{vdw/cc}$ are negative for toluene → benzene transformation, whereas they are positive for aniline → benzene and phenol → benzene transformations. Further, the variation of $\Delta G_{vdw/cc}$ with λ (Figure 16) observed for toluene → benzene transformation corresponds to that observed for typical hydrophobic molecules such as alkanes, whereas the patterns observed for aniline → benzene and phenol → benzene transformations correspond to that of amines. This difference in behavior is consistent with the interaction energy, which decreases for toluene → benzene transformation and increases for the other two transformations. Further, the disappearing group is larger in the first transformation than the latter two cases. These observations suggest that the hydration behavior of aromatic compounds is influenced by the same factors that influence the hydration of aliphatic compounds.

Conclusions

The calculated free energy changes for all the transformations reported here agree reasonably well with the experimental values. The values obtained with the coordinate coupling are in a better agreement with the experimental values than those obtained without the coordinate coupling. In all cases studied, the pattern of free energy variation with mutation of a group of solute atoms is consistent with Frank and Evans' hypothesis of strongly bound solvent structure around the solute. This study supports the view that hydrophobic hydration is a result of the enhanced water structure in the immediate vicinity of the solute. However, the driving force for hydration seems to come from solute–solvent interaction energy which is very large for tetraalkyl- and alkylammonium ions and very small for alkanes.

Acknowledgment. We are grateful to Dr. Richard A. Lerner for providing computational facilities and encouragement. We thank Phyllis Minick for help in correcting the manuscript. This research is partially supported by Grant No. RO1-GM 39410 from NIH.

Registry No. CH_4, 74-82-8; C_2H_6, 74-84-0; C_3H_8, 74-98-6; C_4H_{10}, 106-97-8; Me_4C, 463-82-1; Et_4C, 1067-20-5; Pr_4C, 17312-72-0; Bu_4C, 6008-17-9; NH_3, 7664-41-7; $MeNH_2$, 74-89-5; Me_2NH, 124-40-3; Me_3N, 75-50-3; NH_4^+, 14798-03-9; $MeNH_3^+$, 17000-00-9; $Me_2NH_2^+$, 17000-01-0; Me_3NH^+, 16962-53-1; Me_4N^+, 51-92-3; Et_4N^+, 66-40-0; Pr_4N^+, 13010-31-6; Bu_4N^+, 10549-76-5; C_6H_6, 71-43-2; $C_6H_5CH_3$, 108-88-3; C_6H_5OH, 108-95-2; $C_6H_5NH_2$, 100-46-9; H_2O, 7732-18-5.